LAWRENCE
LIVERMORE
NATIONAL
LABORATORY

UCRL-PROC-222284

Two-Phase Model of Combustion in Explosions

Allen L. Kuhl, Boris Khasainov, John Bell

June 20, 2006

Two-Phase Model of Combustion in Explosions
Karlsruhe, Germany
June 27, 2006 through June 30, 2006

Two-Phase Model of Combustion in Explosions*

Allen L. Kuhl[1], Boris Khasainov[2] & John B. Bell[3]
[1] University of California Lawrence Livermore National Laboratory, Livermore, CA USA
[2] Laboratoire de Combustion et Détonique, UPR 9028 CNRS, 86961 Futuroscope, France
[3] University of California Lawrence Berkeley National Laboratory, Berkeley, CA USA

Abstract

A two-phase model for Aluminum particle combustion in explosions is proposed. It combines the gas-dynamic conservation laws for the gas phase with the continuum mechanics laws of multi-phase media, as formulated by Nigmatulin. Inter-phase mass, momentum and energy exchange are prescribed by the Khasainov model. Combustion is specified as material transformations in the Le Chatelier diagram which depicts the locus of thermodynamic states in the internal energy-temperature plane according to Kuhl. Numerical simulations are used to show the evolution of two-phase combustion fields generated by the explosive dissemination of a powdered Al fuel.

1. Introduction

We consider the explosion of a 0.5-g spherical PETN charge that disperses 1-g of flake Aluminum (Al) powder in a 6.6-l calorimeter as reported by Neuwald [1]. The Al powder is heated by the explosion products, and when the Al mixes with air, it releases 7,400 cal/g by a non-premixed turbulent combustion process [2]. Here we model the evolution of combustion in physical space by numerical simulations.

2. Gas Phase

We model evolution of the combustion field in the limit of large Reynolds and Peclet numbers, where molecular diffusion and heat conduction effects in the gas phase are negligible. The flow field is then governed by the gas-dynamic conservation laws:

Mass: $$\partial_t \rho + \nabla \cdot (\rho \mathbf{u}) = \dot{\sigma}_s \tag{1}$$

Momentum: $$\partial_t \rho \mathbf{u} + \nabla \cdot (\rho \mathbf{u}\mathbf{u} + p) = \rho \mathbf{g} + \dot{\sigma}_s \mathbf{v} - \dot{f}_s \tag{2}$$

Energy: $$\partial_t \rho E + \nabla \cdot (\rho \mathbf{u} E + p\mathbf{u}) = \rho \mathbf{g} \cdot \mathbf{u} - \dot{q}_s + \dot{\sigma}_s E_s - \dot{f}_s \cdot \mathbf{v} \tag{3}$$

where ρ, p, u represent the gas density, pressure and specific internal energy, $\mathbf{u}$ is the gas velocity vector, and $E \equiv u + \mathbf{u} \cdot \mathbf{u}/2$ denotes the total energy of the gas phase. Source terms on the right hand side take into account: mass addition to gas phase due to particle burning ($\dot{\sigma}_s$), gravitational body force ($\mathbf{g}$), particle drag ($\dot{f}_s$), and heat losses ($\dot{q}_s$).

* corresponding author: kuhl2@llnl.gov

3. Particle Phase

We treat the particle phase as continuum. We consider the dilute limit, devoid of particle-particle interactions, so that the pressure and sound speed of the particle phase are zero. We model the evolution of particle phase mass, momentum and energy fields by the conservation laws of continuum mechanics for heterogeneous media as described by Nigmatulin [3]:

Mass: $$\partial_t \sigma + \nabla \cdot \sigma \mathbf{v} = -\dot{\sigma}_s \tag{4}$$

Momentum: $$\partial_t \sigma \mathbf{v} + \nabla \cdot \sigma \mathbf{v}\mathbf{v} = \sigma \mathbf{g} - \dot{\sigma}_s \mathbf{v} + \dot{f}_s \tag{5}$$

Energy: $$\partial_t \sigma E_s + \nabla \cdot \sigma E_s \mathbf{v} = \sigma \mathbf{g} \cdot \mathbf{v} + \dot{q}_s - \dot{\sigma}_s E_s + \dot{f}_s \cdot \mathbf{v} \tag{6}$$

Number particles: $$\partial_t n_s + \nabla \cdot n_s \mathbf{v} = 0 \tag{7}$$

where σ and $\mathbf{v}$ represent the particle phase density and velocity while $E_s \equiv C_s T_s + \mathbf{v} \cdot \mathbf{v}/2$ denotes the total energy of the particle phase.

4. Inter-Phase Interaction Terms [4]

Mass Exchange: $$\dot{\sigma}_s = \begin{cases} 0 & T_s < T_{ign} \\ -3\sigma(1 + 0.276\sqrt{\mathrm{Re}_s})/t_s & T_s \geq T_{ign} \end{cases} : \tag{8}$$

Empirical Burning Law: $$t_s = K d_{s0}^n / \phi^{0.9} \tag{9}$$

Momentum Exchange: $$\dot{f}_s = \frac{3}{4}\frac{\rho}{\rho_s}\frac{\sigma}{d_s} C_D (\mathbf{u} - \mathbf{v})|\mathbf{u} - \mathbf{v}| : \tag{10}$$

$$\text{where} \quad C_D = \frac{24}{\mathrm{Re}_s} + \frac{4.4}{\sqrt{\mathrm{Re}_s}} + 0.42 \qquad \& \qquad \mathrm{Re}_s = \rho d_s |\mathbf{u} - \mathbf{v}|/\mu \tag{11}$$

Heat Exchange: $$\dot{q}_s = \frac{6\sigma}{\rho_s d_s}\left[\frac{Nu\lambda(T - T_s)}{d_s} + \varepsilon\sigma_{Boltz}(T^4 - T_s^4)\right] \;\&\; Nu = 2 + 0.6\,\mathrm{Pr}\sqrt{\mathrm{Re}_s} \tag{12}$$

5. Combustion Model

We consider three components: air (*A*), fuel (*F*) consisting of Al vapor, and equilibrium combustion products (*P*). They are governed by the following conservation laws:

Air-A: $$\partial_t \rho Y_{Air} + \nabla \cdot \rho Y_{Air} \mathbf{u} = -\alpha_s \dot{\sigma}_s \tag{13}$$

Fuel-F (metal vapor): $$\partial_t \sigma_F + \nabla \cdot \sigma_F \mathbf{u} = -\dot{\sigma}_s \tag{14}$$

Products-P: $$\partial_t \rho Y_P + \nabla \cdot \rho Y_P \mathbf{u} = (1 + \alpha_s)\dot{\sigma}_s \tag{15}$$

These are augmented by the conserved scalar equation:

Conserved Scalar: $$\partial_t (\sigma_F + \rho Y_{Air}) + \nabla \cdot (\sigma_F + \rho Y_{Air})\mathbf{u} = 0 \tag{16}$$

Fuel and air are consumed in stoichiometric proportions: $\alpha_s = air/fuel = 4.03$.

6. Thermodynamics

The thermodynamic states encountered during the combustion of the aluminum powder with air are depicted in Fig. 1: the Le Chatelier diagram of Kuhl [5,6]. The Reactants-R are

defined as a stoichometric mixture of air and Aluminum in *frozen* composition (air/fuel ratio: $\alpha_s = 4.03$). The Products-P are assumed to be in *thermodynamic equilibrium*. These states were calculated with the Cheetah code, assuming $p = 1 atm$. Computations were also performed assuming combustion at $p = 10 atm$; the resulting curve was negligibly different from the 1-atm curve for temperatures below 3,500K, so the 1-atm curve was adopted as the standard for this problem. Pressure independence of the $u(T)$ curve is a perfect gas property, which seems to apply for the present combustion conditions. The heat of combustion is the difference between the energy of the products minus energy of reactants: $H_c \equiv u_{0,P} - u_{0,R} = -1{,}473 cal/g_P$ $(7{,}409 cal/g_{Al})$ and is indicated on Fig. 1. Adiabatic combustion corresponds to a material transform from Reactants to Products at constant energy. For Reactants starting at 300 K, this gives a combustion temperature of 3,680 K, as indicated in the figure. These states have been fit with quadratic functions:

$$u_k(T) = a_k T^2 + b_k T + c_k \qquad (k = A, DP, R, P) \tag{17}$$

These functions (curves) do an excellent job at fitting the computed thermodynamic states (data points) as demonstrated in Fig. 1.

The pressure variation with specific volume along the CJ insentrope was computed with the Cheetah code. This $p - \mathrm{v}$ relation is fit with the Jones-Wilkins-Lee (JWL) function:

$$p_{JWL}(\mathrm{v}, S_{CJ}) = A \exp(-R_1 \mathrm{v}) + B \exp(-R_2 \mathrm{v}) + \frac{C}{\mathrm{v}^{1+\omega}} \tag{18}$$

where v represents the specific volume ratio: $\mathrm{v} = v/v_0$. For PETN at $\rho_0 = 1 g/cc$, the JWL constants are A=5.80227 M-bar; B=0.09301 M-bars; C=0.01223 M-bars; $R_1 = 7.000$; $R_2 = 1.695$ and $\omega = \gamma - 1 = 0.246$. For $v > 28 cm^3/g$, these *p* values lie on the line $pv/RT = 1$ representing the perfect gas law. This leads to the following relation for the DP gases:

$$p = \begin{cases} p_{JWL}(\mathrm{v}, S_{CJ}) & \mathrm{v} \le 28 \mathrm{cm}^3/g \\ \rho_m R_m T_m & \mathrm{v} > 28 \mathrm{cm}^3/g \end{cases} \tag{19}$$

For computational cells containing a mixture of components, the perfect gas mixing relations are used, so the mixture temperature is calculated from:

$$T_m = [-b_m + \sqrt{b_m^2 - 4 a_m (c_m - u_m)}]/2a_m \tag{20}$$

representing an inversion of (17), and the mixture properties are determined from:

$$a_m = \sum_k Y_k a_k, \; b_m = \sum_k Y_k b_k, \; c_m = \sum_k Y_k c_k, \; R_m = \sum_k Y_k R_k \tag{21}$$

7. Results

Numerical simulations of the explosion of an Al-SDF charge (0.5-g PETN +1.0-g flake Al) in a 6.6-liter calorimeter were performed. The two-phase fields are complicated enough, so for clarity, we approximate the problem as 1-D spherical, and assume that gravity $\mathbf{g} = 0$. The evolution of the gas and particle fields of velocity, density and temperature are presented in Fig. 2, for times covering the period before first reflection of the blast wave from the calorimeter wall. The corresponding slip velocity and slip temperature fields and the drag force are depicted in Fig. 3. Figure 4 provides the evolution of the pressure field, along with the burning rate and the inter-phase heat transfer. Evolution of the Reynolds number and Damköhler number profiles are shown in Fig. 5. The evolution of mass fraction fields of air and fuel (Al) are presented in Fig. 6, along with the equilibrium species profiles at late times.

8. Discussion

Inter-phase slip velocities are large (800 *m/s*). Initially the gas accelerates the particle phase, but later the particles accelerate the gas. Gas temperatures in the combustion cloud reach 3,000 *K*, while the particle phase temperature quickly attains the melting temperature of 933 *K*, and then the ignition temperature of 1,000 *K*; later the gas heats particles to 2,500 *K* due to the large inter-phase slip temperatures (1,500 K). The explosion drives a blast wave of 10 bars all the way to the chamber wall ($r = 11.3cm$). Although the flow velocities induced by the explosion are in the range of 1-2 *km/s*, the Reynolds numbers (based on the slip velocity and mean particle diameter: $d = 4.3\mu m$) are very small ($Re < 1$)—indicative of the *Stokes-flow regime*. Damköhler numbers are also very small ($Da \approx 0.003$)—corresponding to the *distributed-combustion regime*; nevertheless, more than 95% of the fuel is consumed in 1 ms (Fig. 7a). Combustion of Al in air results in many products species; the major species (Al_2O_3 liquid & solid, AlO, Al_2O, Al_2O_2, AlO_2, etc.) are shown in Fig. 6; it also indicates the persistence of electron concentrations in the combustion cloud to late times (5 ms).

A numerical simulation was also performed for an un-confined Al-SDF explosion. Results are presented in Fig. 7, and compared with waveforms from the confined case at the same times (1 & 2 ms). Although the blast waves are quite different (Fig. 7b), the combustion cloud temperatures are similar ~ 3,500 K, corresponding to the adiabatic flame temperature of the mixture. In the un-confined explosion, the combustion cloud expands to about twice the radius of the 6.6-liter chamber, but maintains a high temperature due to combustion, even though about 20% of the Al fuel remains un-burned in this theoretical simulation.

9. Conclusions

According to these simulations, one can characterize this problem as distributed combustion ($Da << 1$) of Al particles in the Stokes flow regime ($Re < 1$). This illustrates that the particle phase acts as an *ensemble*—causing the mixture to behave, in effect, like a viscous continuum. In our formulation, we treat the particle phase variables as *Eulerian fields* obeying the conservation laws of mechanics of heterogeneous continuous media. This continuum formation highlights the ensemble effects of the particles on the flow, and is more efficient than other formulations (e.g. particle methods) for this problem.

The thermodynamic formulation used here, whereby combustion is modeled as material transformations in the Le Chatelier plane, provides a simpler description of thermodynamic states in the case of lean mixtures and low pressures, than our previous tabulated EOS model [5]. And being analytic, it is inherently faster than table look-up methods.

10. References

[1] P. Neuwald, H. Reichenbach and A. L. Kuhl 2003 "Shock-Dispersed Fuel Charges—Combustion in Chambers and Tunnels", *Energetic Materials*, 34th ICT Conf, 13.1-13.14.

[2] A. L. Kuhl, R. E. Ferguson and A. K. Oppenheim 1999 "Gas-dynamics of Combustion of TNT Products in Air", *Archivum Combustionis* 19:1-4, 67-89.

[3] R. I. Nigmatulin, **Dynamics of Multi-phase Flows**. Vol. 1. Moscow: Nauka, 1987, 464p.

[4] B. Khasainov, A. L. Kuhl, S. Victorov and P. Neuwald 2005 "Model of Non-Premixed Combustion of Al-Air Mixtures" *14th APS Meeting on Shock Compression of Condensed Matter*, American Physical Society (in press).

[5] A. L. Kuhl, M. Howard and L. Fried 1999 "Thermodynamic Model of Afterburning in Explosions" *Energetic Materials*, 34th ICT Conference, 74.1-74.14.

[6] A. L. Kuhl, 2006 "Thermodynamic Model of Aluminum Combustion in SDF Explosions", *Energetic Materials*, 37th ICT Conference, Karsruhe, Germany.

Acknowledgements

This work was performed under the auspices of the U. S. Department of Energy by the University of California, Lawrence Livermore National Laboratory under Contract No. W-7405-Eng-48. It was sponsored by the Defense Threat Reduction Agency under IACRO # 05-4071.

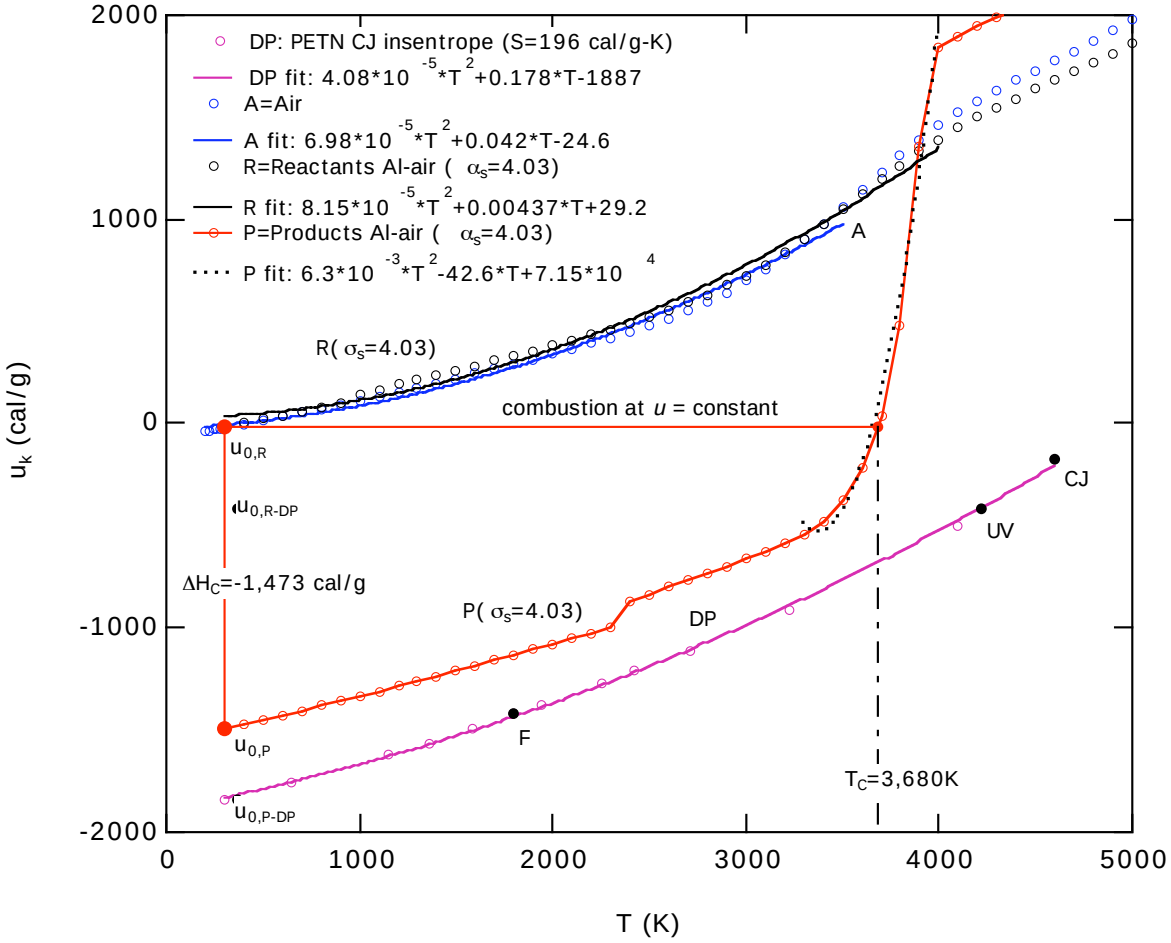

Figure 1. Le Chatelier diagram for stoichiometric combustion of aluminum in air ($\alpha_s = 4.03$). Adiabatic combustion corresponds to a material transformation from the Reactants-R to the Products-P at constant energy, represented as a horizontal line shown for reactants at 300K. The points are calculated with the Cheetah code, and fit with the quadratic EOS functions: $u_k(T) = a_k T^2 + b_k T + c_k$ (see insert in figure).

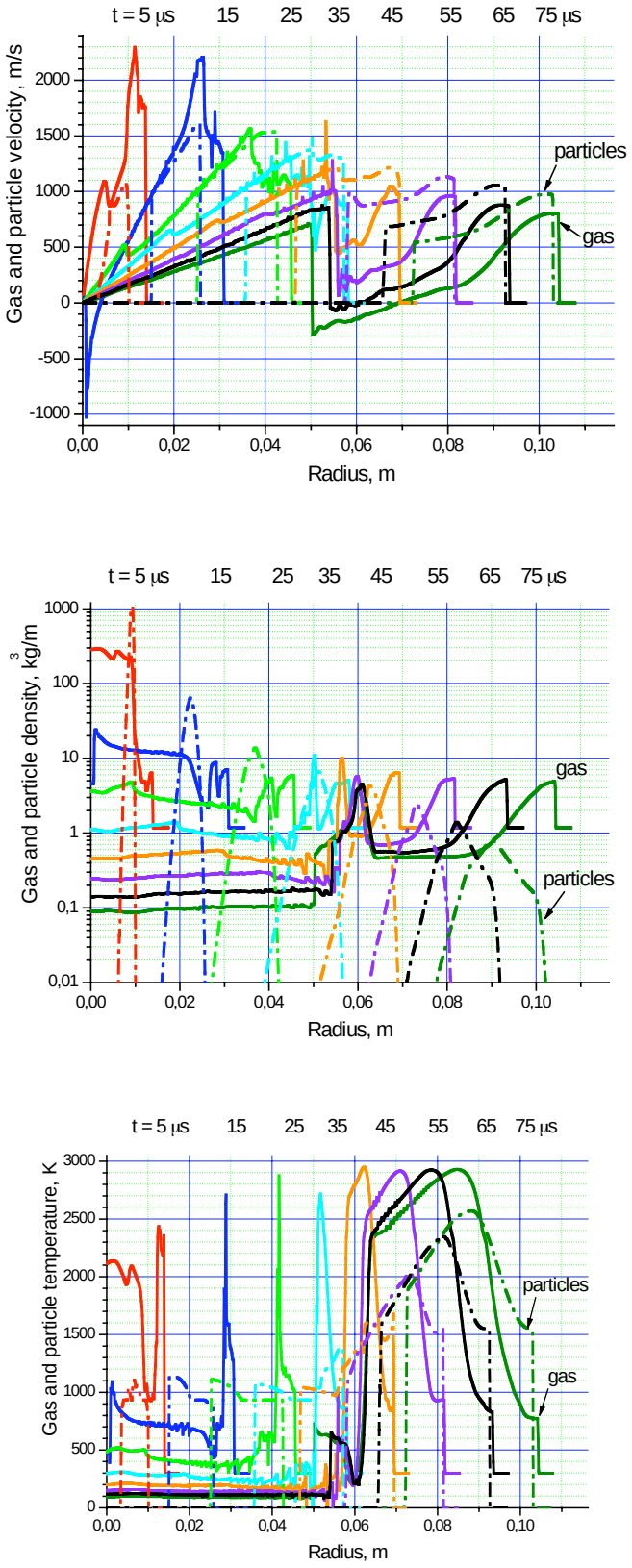

Figure 2. Evolution of flow field during the blast wave expansion: (a) velocity, (b) density, and (c) temperature profiles. Dashed lines denote particle phase.

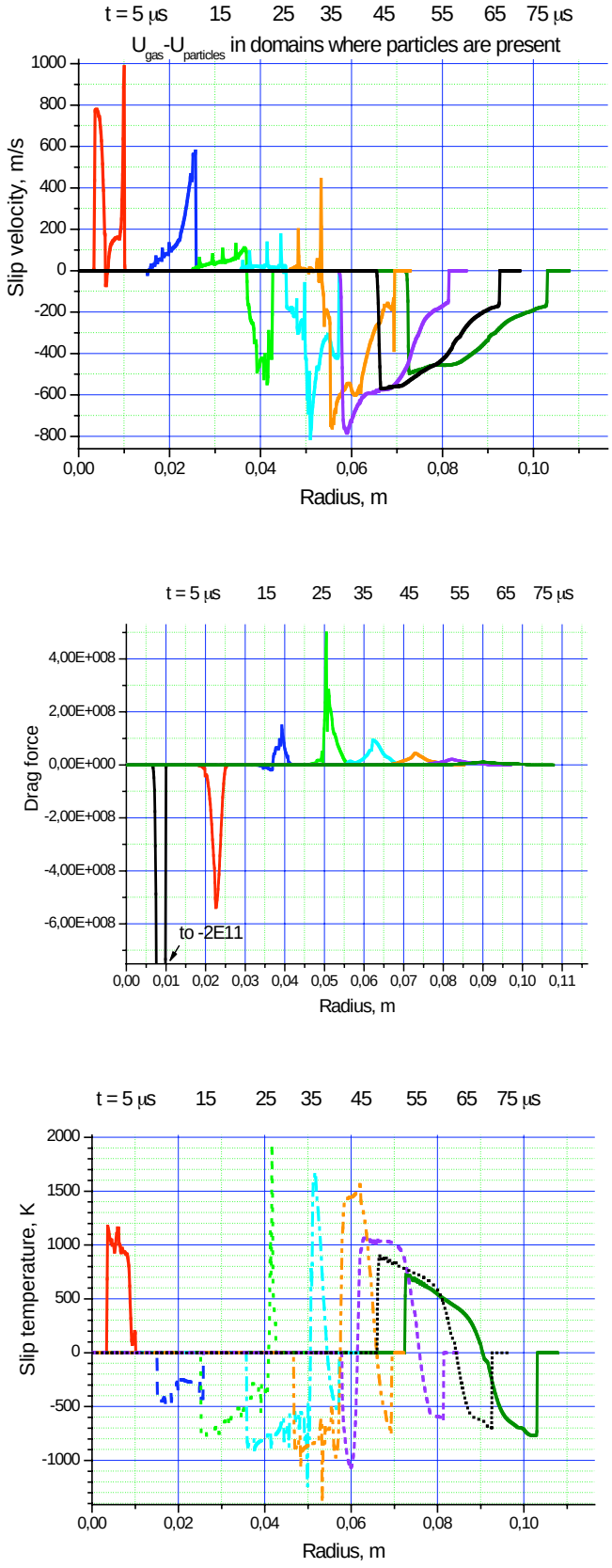

Figure 3. Evolution of the flow field during the blast wave expansion: (a) slip velocity, (b) drag force per unit volume, kg/(m-s)^2, (c) slip temperature.

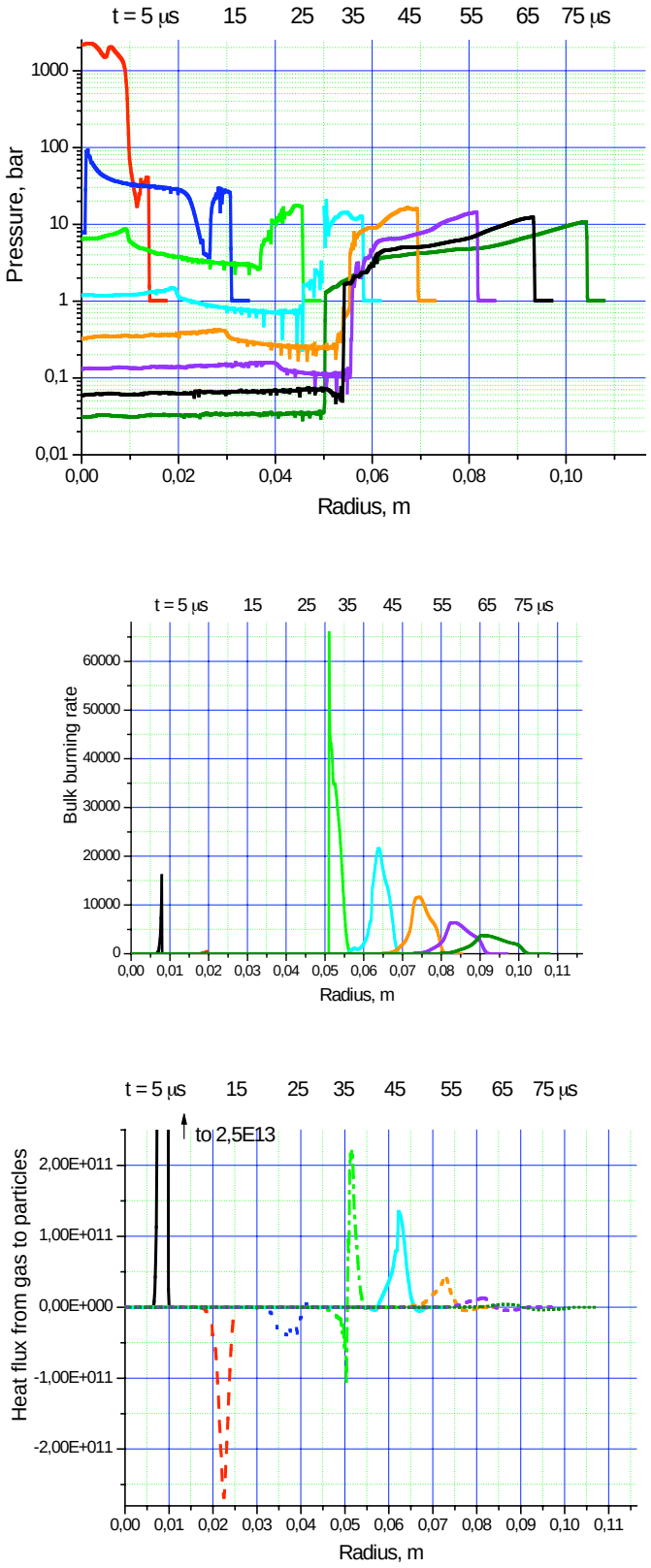

Figure 4. Evolution of the flow field during the blast wave expansion: (a) pressure, (b) bulk burning rate per unit volume kg/(s-m^3), (c) heat flux from the gas to particle phase per unit volume J/(s-m^3).

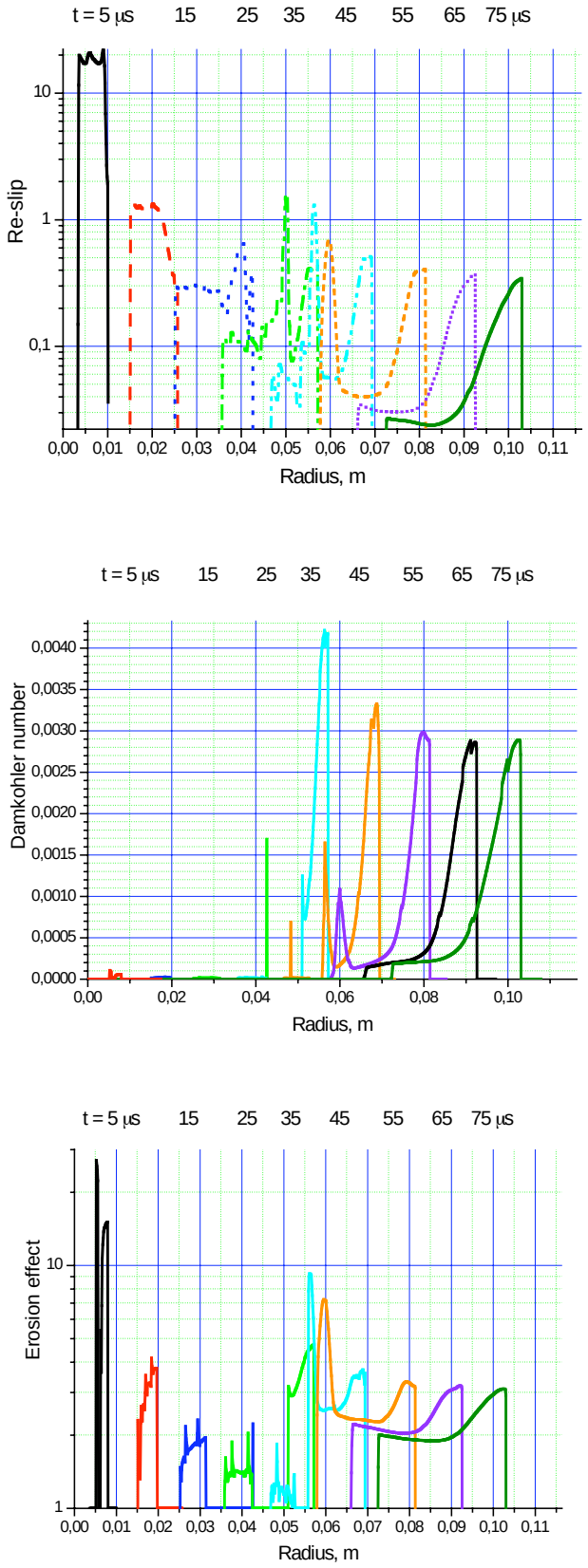

Figure 5. Evolution of the flow field during the blast wave expansion: (a) Reynolds number profiles, (b) Damköhler number profiles, (c) erosion effect.

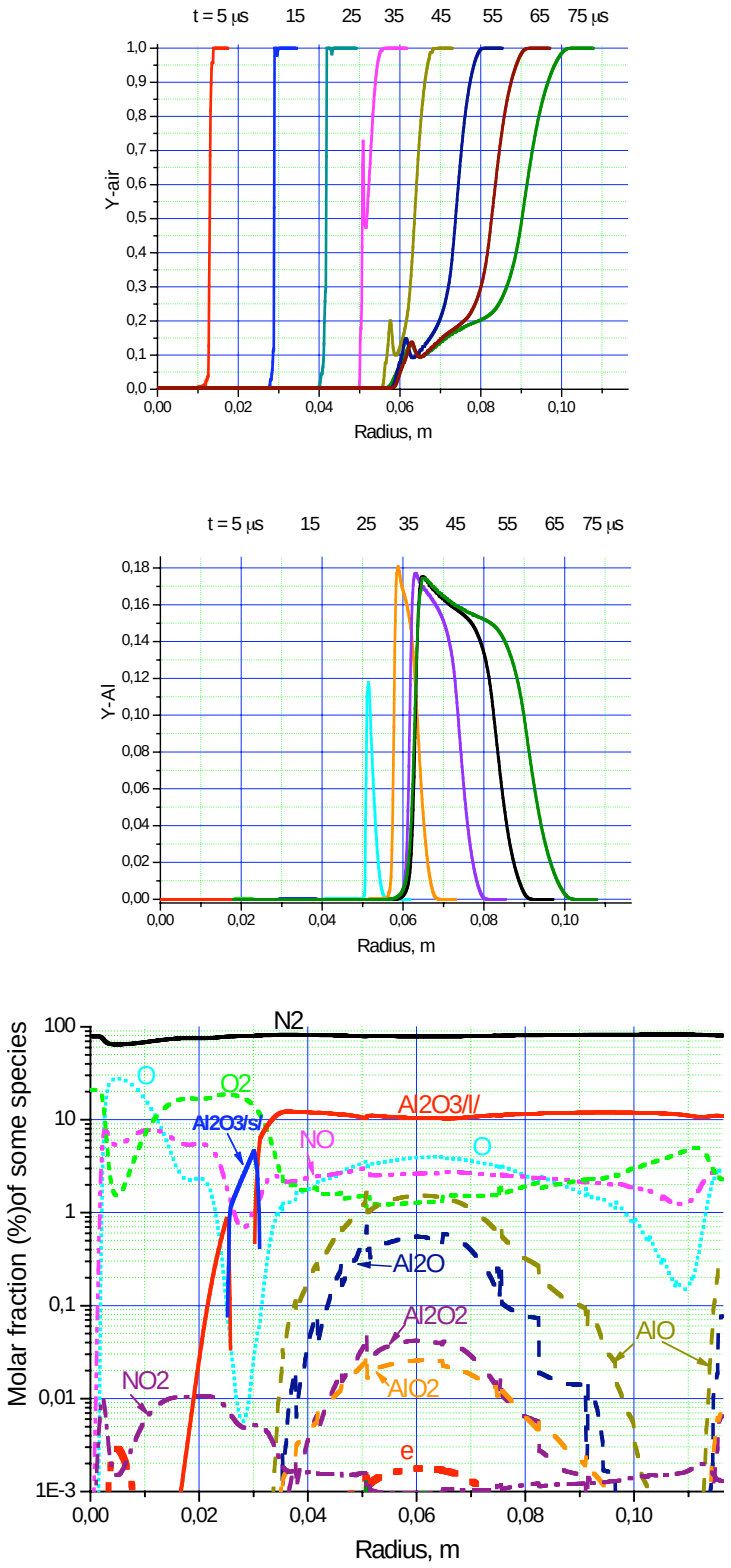

Figure 6. Evolution of the mass fraction profiles during the blast wave expansion: (a) air profiles, (b) Al (in combustion products) profiles, (c) species profiles at 5 ms.

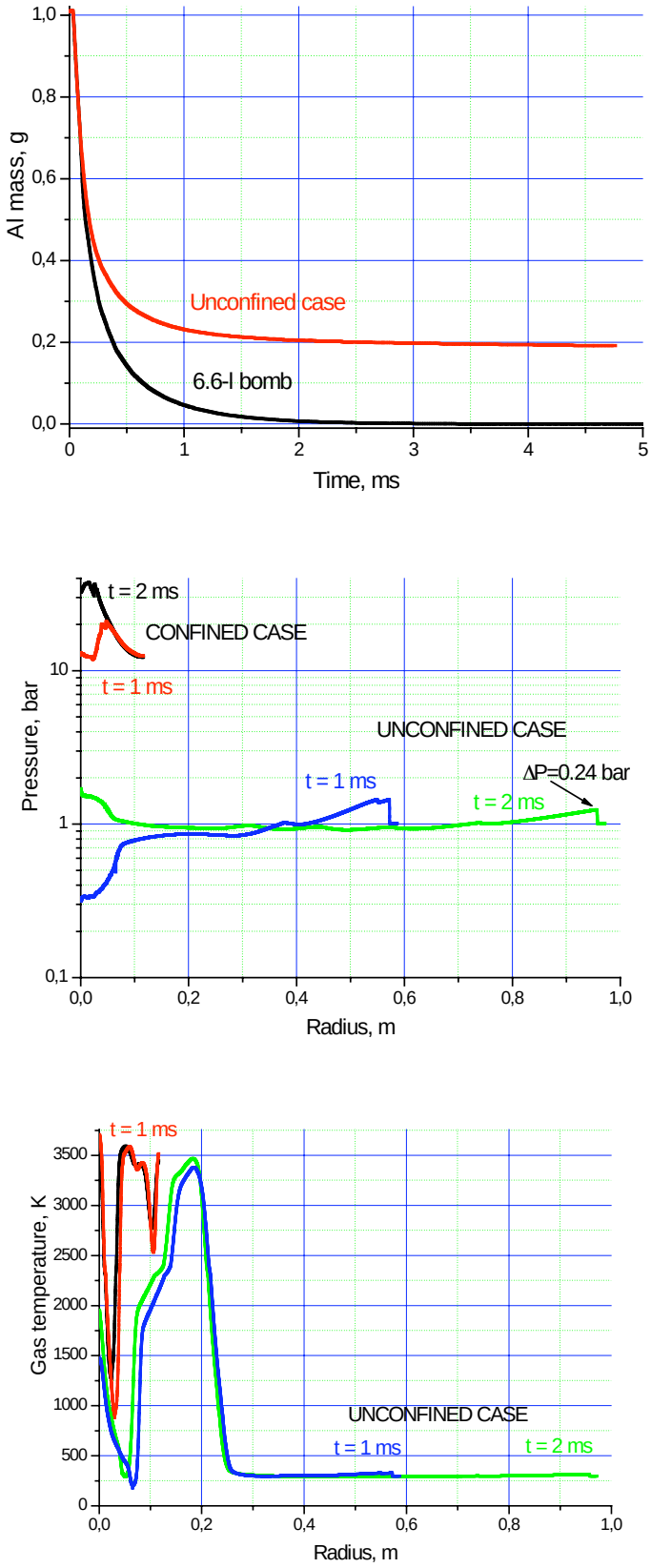

Figure 7. Comparison of results from simulations of confined (6.6-liter bomb) and unconfined explosions: (a) Al fuel history, (b) pressure profiles, (c) temperature profiles.